Appl. Phys. B 42, 129–145 (1987)

Applied Physics B Photophysics and Laser Chemistry

Standard and Phase-Matched Grazing-Incidence and Distributed-Feedback FIR Gas Lasers

D. Wildmann, S. Gnepf, and F. K. Kneubühl

Infrared Physics Laboratory, Institute of Quantum Electronics, ETH, CH-8093 Zürich, Switzerland

Received 16 September 1986/Accepted 17 November 1986

Abstract. In this paper we review theoretical and experimental studies on optically pumped 496 μm CH_3F DFB lasers of different configurations, including grazing-incidence arrangement and phase matching by a gap in the periodic structure. These configurations combine the simple tuning mechanism of grazing-incidence systems with the high frequency selectivity of DFB. Our theoretical considerations based on coupled-wave theory are concerned with the dispersion relations and resonance conditions of standard and phase-matched DFB and grazing-incidence gas lasers. We have succeeded in calculating the relevant TM coupling coefficients for lasers with rectangular periodic waveguides. For laser cavities with various continuous gratings we have measured the resonant heights and tuning angles of the laser oscillations of first- and second-order DFB. We have found good agreement with theoretical resonance conditions. In order to improve the mode selectivity and to attain single longitudinal mode operation, which is a requirement for semiconductor lasers in many applications, we have introduced variable gaps in the center of the gratings. These provide phase matching and gap modes. We have compared the measured gap modes with our theory and found agreement in specific cases, where the phase-matched cavity implies single-mode laser operation. Our results on standard and phase-matched DFB cavities promise an improvement of the performance of phase-matched semiconductor lasers with respect to small bandwidth and optimized output power.

PACS: 42.60B, 42.60D, 42.80F, 42.80L

1. Introduction

1.1. Grazing-Incidence Dye Lasers

Gratings at grazing-incidence in pulsed dye lasers were first introdiced by Shoshan et al. [1], Littman [2, 3], and Metcalf [3]. The goals of this new cavity design was simplicity and narrow-band operation without intracavity beam expander [4]. Grazing-incidence was chosen in order to illuminate the full width of the diffraction grating which is required for narrow-band operation. Figure 1 shows a schematic view of the cavity design. The cavity is formed by a grating and a tuning mirror. The output mirror is either partially [3] or totally [1] reflecting. In the latter case, the zero-order reflection from the grating is used for output coupling. Later, the grazing-incidence cavity was modified by Saikan [5] who introduced a resonant mirror instead of the full reflector, and by Dinev et al. [6, 7] with the aid of a double grazing-incidence arrangement. Recently, the grazing-incidence arrangement was further improved by Lin and Littman [8], Littman [9], and McNicholl and Metcalf [10]. They proposed a synchronous cavity mode and feedback wavelength scanning in grazing-incidence lasers.

1.2. Distributed and Helical Feedback Lasers

Distributed Feedback (DFB) was first incorporated in dye lasers [11, 12]. In DFB lasers the conventional resonator mirrors are replaced by a periodic structure, which provides a frequency selective feedback related to the Bragg effect. Later, Nakamura et al. [13]

realized DFB in a semiconductor laser. Laser diodes with periodic DFB structures as well as with distributed Bragg reflectors (DBR) have been extensively studied [14] because of their frequency selectivity. An important feature of DFB and DBR semiconductor lasers is the compatibility with the planar fabrication process. First operation of a DFB gas laser was finally achieved in 1979 and subsequently studied in detail [15–18]. This DFB gas laser is an optically pumped 496 μm CH_3F laser [19] equipped with a periodically modulated waveguide cavity.

The first theory on DFB lasers presented by Kogelnik and Shank [20] is based on the coupled-mode theory of an active medium of finite length with weakly modulated periodic index and/or gain. In the past years the theory on DFB lasers has been considerably improved by Gnepf and Kneubühl [21–23], who also included strong index, gain and combined periodic modulations.

Recently, Preiswerk et al. [24–26] performed an extensive group theoretical and experimental study on distributed and helical feedback in lasers. Thus, they succeeded in the operation of the first helical feedback (HFB) laser, an optically pumped 496 μm CH_3F laser with a helical waveguide.

With the intention to remove the mode degeneracy of conventional DFB lasers by introducing a gap in the periodic structure, Shubert [27] developed a theory for DFB lasers with nonuniform gain and coupling. A similar study was made by Haus and Shank [28] by introduction of an antisymmetric taper of the coupling coefficient. In the USSR calculations on fields and transmission properties of helical and linear periodic corrugated metal waveguides were carried out by Kovalev et al. [29], Denisov and Reznikov [30], and Bratman et al. [31] on the basis of the perturbation theory developed by Katsenelenbaum [32]. These authors also proposed corrugated metal waveguides with a gap in the middle of the corrugation. Kim and Fonstad [33] presented theoretical and experimental considerations on narrowband optical thin-film filters with integrated gap. Later, Sekartedjo et al. [34] reported on a DBR semiconductor laser with phase adjustement by a gap in the corrugation. Recently, a new design of a DBR laser has been proposed in order to favor the gap mode by a high- and a low-reflecting end of the cavity [35]. In addition, an optimized $\frac{\pi}{2}$ distributed feedback laser in the 1.5 μm wavelength region was devised by McCall and Platzman [36].

1.3. Grazing-Incidence Gas Lasers

The first optically pumped DFB gas laser was tuned by a variation of the groove spacing. This was realized by a temperature variation of the corrugated waveguide [15–17]. In order to simplify the tuning mechanism of this type of lasers, we have developed a grazing-incidence gas laser as modification of the DFB gas laser [37–43]. In order to incorporate the grazing-incidence arrangement in gas lasers working at far-infrared (FIR) wavelengths, several modifications of the grazing-incidence dye laser scheme had to be worked out. First of all, a waveguide configuration had to be introduced in order to eliminate diffraction losses. Furthermore, efficient feedback was only attained by a small separation of the order of a few FIR wavelengths between grating and tuning mirror. This implies Fresnel instead of Fraunhofer diffraction. Because of the well-known difficulties with the Fresnel diffraction formalism, we have replaced it by a theory including waveguiding and DFB.

The theory of standard and phase-matched DFB and grazing-incidence gas lasers is presented in Sects. 2–4. In Sect. 2 we discuss the coupled-wave theory of DFB, the characteristics of wedged waveguides and the evaluation of coupling coefficients of corrugated metallic waveguides of rectangular cross section. These three items are the prerequisite for an understanding of the basic properties of DFB and grazing-incidence gas lasers. Their dispersion relations and resonance conditions are elucidated in Sect. 3 with the assumption, that the laser cavities include only continuous gratings which do not provide phase matching. The resonance condition for lasers with phase matching by a gap in the center of the grating is the topic of Sect. 4.

Design and operation of the first standard and phase-matched grazing-incidence DFB gas laser are described in Sect. 5, while Sect. 6 presents the resonances measured with three different continuous gratings which exhibit first- as well as second-order DFB. Section 7 is devoted to the first-order DFB resonances in the bandgap, which have been observed when a variable gap was introduced in the center of the cavity gratings. Finally, we summarize in Sect. 8 our conclusions drawn from theory and experiments with the standard and phase-matched DFB and grazing-incidence gas lasers.

2. Perturbation Theory

2.1. General DFB Theory

Theories for DFB lasers are concerned with the calculation of dispersion relations, resonance frequencies, threshold gains, and DFB mode couplings. These properties can be derived from the basic wave equation of the amplitude $E(z)$ of the oscillating electric field

$$E(z,t)=E(z)\exp(+i\omega t) \tag{1}$$

as a function of the position z in the DFB structure [20]

$$\frac{d^2E(z)}{dz^2}+K^2(z)\,E(z)=\frac{d^2E(z)}{dz^2}+V(z)\,E(z)=0. \tag{2}$$

The wavenumber $K(z)$ and the "potential" $V(z)$ are periodic

$$K(z)=K(z+L)=K(z+\pi/\beta_0),\ \beta_0=\pi/L. \tag{3}$$

L denotes the period of the DFB structure, and β_0 the Bragg wavenumber. For a periodic structure without loss or gain, $K(z)$ as well as $V(z)$ are real. Consequently, (2) corresponds to the Schrödinger equation of an electron in a one-dimensional periodic potential. On the other hand, $K(z)$ and $V(z)$ are complex for an active DFB structure. In this case $K(z)$ is usually approximated by

$$K(z)=c^{-1}\omega n(z)+\mathrm{i}\alpha(z)=K(z+L), \tag{4}$$

where the periodic gain $\alpha(z)$ and the periodic effective refractive index $n(z)$ are assumed to be independent of the angular frequency ω.

With the complex wavenumber (4) Eq. (2) represents a Hill differential equation [44–46]. While the solutions of Hill equations with real periodic potentials $V(z)$ are well established, little is known about the solutions of Hill equations with complex periodic potentials. Recently, Gnepf and Kneubühl [21, 22] presented a comprehensive theory on DFB lasers based on the complex Hill equation, which includes weak as well as strong periodic index, gain and combined modulations.

2.2. *Coupled-Wave Theory*

Coupled-wave theory was first applied to DFB lasers by Kogelnik and Shank [20]. Subsequently, this theory has been refined and extended by several authors, e.g. by Marcuse [47, 48], Kogelnik et al. [49], Wang [50–53], Yariv [54, 55], and Gover [55].

For TEM waves in dielectric bulk media [20] or guided TE waves in slab-type dielectric waveguides [47, 56] the electric field $E(z,t)$ can be represented as a summation over all the discrete modes which may propagate in the unperturbed waveguide. In coupled-wave theory the considerations are often restricted to a combination of two counterpropagating guided modes characterized by the propagation constants $\beta_\pm$. Therefore, we assume that for TE waves, the amplitude $E(z)$ of the electric field determined by the wave equation (2) can be split into two counterpropagating waves according to Shubert [27]

$$E(z)=c_+(z)\exp(-\mathrm{i}\beta_+z)+c_-(z)\exp(-\mathrm{i}\beta_-z), \tag{5}$$

where $c_\pm$ are the amplitudes of the guided modes propagating in $\pm z$ direction. In addition, we assume weak periodic index and gain modulations

$$\begin{aligned} n(z)&=n+n_1\cos(2\beta_0z),\\ \alpha(z)&=\alpha+\alpha_1\cos(2\beta_0z), \end{aligned} \tag{6}$$

where $|\alpha|,\ k|n_1|\ll kn$

$$k=\omega/c=2\pi/\lambda_{\text{free space}}. \tag{7}$$

Conditions (7) imply the following approximation [20] for the characteristic wavenumber $K(z)$ of wave equation (2)

$$\begin{aligned} K^2(z)\cong\ & kn(kn+2\mathrm{i}\alpha)\\ &+2kn(kn_1+\mathrm{i}\alpha_1)\cos(2\beta_0z). \end{aligned} \tag{8}$$

In this study we neglect gain modulation: $\alpha_1=0$. In a first approximation the substitution of (5 and 8) in the wave equations yields the coupled-wave equations

$$\begin{pmatrix} dA_+/dz\\ dA_-/dz\end{pmatrix}=\begin{pmatrix} -\mathrm{i}(\Delta+\mathrm{i}\alpha) & -\mathrm{i}\kappa_+\\ \mathrm{i}\kappa_- & \mathrm{i}(\Delta+\mathrm{i}\alpha)\end{pmatrix}\begin{pmatrix} A_+\\ A_-\end{pmatrix} \tag{9}$$

with

$$\begin{aligned} A_+&=c_+\,\mathrm{e}^{-\mathrm{i}\Delta z},\\ A_-&=c_-\,\mathrm{e}^{+\mathrm{i}\Delta z}. \end{aligned} \tag{10}$$

The parameter Δ is the detuning factor relative to the Bragg wavenumber β_0

$$\Delta=(\beta_+-\beta_--2\beta_0)/2. \tag{11}$$

The coupling coefficients $\kappa_\pm$ represent a measure for the strength of the Bragg scattering (Sect. 2.4).

An adequate general solution of (9) consists of a linear combination of two counterpropagating eigenwaves

$$\begin{pmatrix} A_+\\ A_-\end{pmatrix}=a_+\begin{pmatrix} 1\\ s_+\end{pmatrix}\exp(-\mathrm{i}\gamma z)+a_-\begin{pmatrix} s_-\\ 1\end{pmatrix}\exp(\mathrm{i}\gamma z) \tag{12}$$

with the constant amplitudes $a_\pm$, and the components

$$s_\mp=-\kappa_\pm/(\Delta+\mathrm{i}\alpha+\gamma). \tag{13}$$

The propagation constant γ is determined by the dispersion relation

$$\gamma^2=(\Delta+\mathrm{i}\alpha)^2-\kappa_+\kappa_-. \tag{14}$$

For positive gain α, we define the sign of the propagation constant γ such that $\mathrm{Im}\{\gamma\}>0$.

Solution (12) fulfils the condition that for vanishing coupling coefficients $\kappa_\pm$ the (A_+, A_-) represent the unperturbed waves, i.e. a linear combination of two counterpropagating unperturbed waves with gain or loss α. Furthermore, the components $s_\pm$ show no singularities for any Δ or $\kappa_\pm$.

2.3. Waveguide Characteristics

The cavities of our lasers consist of slightly wedged hollow metallic waveguides of rectangular cross section. The propagation of electromagnetic modes in a hollow metallic waveguide is determined by the dispersion relation [57]

$$\beta_{mn}^2 = k^2 - k_{c,mn}^2, \tag{15}$$

where β_{mn} is the propagation constant, and $k_{c,mn}$ the characteristic cutoff wavenumber of the mode labeled by m and n. For a wedged waveguide $k_{c,mn}$ depends on the position z on the waveguide axis

$$k_{c,mn}^2 = [\pi n/(2a + z \cdot \sin\Phi)]^2 + (\pi m/2b)^2, \tag{16}$$

where $2b$ denotes the total width and $2a$ the total height at $z=0$ of the waveguide. Φ is the angle of inclination or the tuning angle. Thus, the propagation constant β_{mn} of a certain mode mn also depends on z.

In order to determine a resonance condition for a wedged waveguide, the z dependence of the propagation constant must be eliminated. This is realized by an integration over a whole round trip which represents an averaging process of the propagation constant [58]. Assuming that $\beta_+(z)$ denotes a wave in forward direction and $\beta_-(z)$ a wave in the backward direction we write

$$(\beta_+ - \beta_-) = \frac{1}{R}\int_0^R [\beta_+(z) - \beta_-(z)]\, dz \tag{17}$$

with

$$\begin{aligned} &\beta_+(z) > 0, \\ &\beta_-(z) < 0, \end{aligned} \tag{18}$$

R being the length of the waveguide. In the following we shall replace $(\beta_+ - \beta_-)$ by the average defined as the right side of (17). For small tuning angles Φ we have justified this procedure experimentally (Sects. 6 and 7).

As previously mentioned, we assume a constant gain α, i.e. pure index modulation. We can split the gain α into the proper gain α^{gain} due to the active laser medium and the loss $\alpha_{mn}^{\text{loss}}$ due to the waveguide losses which depend on the mode mn

$$\begin{aligned} &\alpha = \alpha^{\text{gain}} + \alpha_{mn}^{\text{loss}}, \\ &\alpha^{\text{gain}} \geqq 0;\ \alpha_{mn}^{\text{loss}} \leqq 0. \end{aligned} \tag{19}$$

The loss $\alpha_{mn}^{\text{loss}}$ of the mode nm is determined by the skin depth

$$\delta_s = [2/(kZ_0\sigma)]^{1/2}, \tag{20}$$

where $Z_0 = 377\ \Omega$ represents the free-space impedance of vacuum, and σ the electrical conductivity of the walls. For a rectangular waveguide of height $2a$ and width $2b$ the loss $\alpha_{mn}^{\text{loss}}$ of mode mn is given by

$$\alpha_{mn}^{\text{loss}} = -k^2\delta_s/(2\beta_{mn}) \times (n^2/a^3 + m^2/b^3)/(n^2/a^2 + m^2/b^2). \tag{21}$$

2.4. Coupling Coefficients

The coupling coefficients $\kappa_\pm$ are crucial parameters of the coupled-wave theory because they determine the relative power per unit length exchanged between the two modes. While there is a general agreement in literature about the coupling coefficients for TE polarization [27, 59–63], there are conflicting results with regard to the coupling coefficients for TM polarization [48, 59, 64] depending on the analytical approach. Fortunately, the essential features of backward Bragg coupling in DFB lasers can be observed without considering in detail the coupling between modes of the discrete spectrum [27].

In contrast to Shubert [27], Kogelnik and Shank [20] considered two coupled bulk waves propagating in a dielectric medium, i.e. $\beta_+ = -\beta_- = \beta$. This implies rather simple coupling coefficients

$$\kappa_+ = \kappa_- = \kappa = (\beta_0 n_1/n + i\alpha_1)/2 \tag{22}$$

independent of β. Recently, Gnepf and Kneubühl [22] calculated the TEM coupling for strong index and/or gain modulation. In a waveguide however, a coupling between different forward (β_+) and backward (β_-) modes is also possible [27]. In this case, the coupling coefficients have to be calculated by overlap integrals of the transverse fields of the proper modes. Yet, all these calculations refer to the coupled-wave theory of TEM bulk waves or TE and TM waves in dielectric media.

A coupled-wave theory which allows the calculation of coupling coefficients for modes in metallic waveguides was developed by Katsenelenbaum [32]. Subsequently, it was extended by Kovalev et al. [29], Denisov and Reznikov [30], and Bratman et al. [31]. In order to describe the perturbations in a hollow metal waveguide, Katsenelenbaum [32] introduced a magnetic surface current j^m. For this purpose he modified the relevant Maxwell equation as follows

$$\text{curl}\,\mathbf{E} = -\mu_0\, \partial/\partial t\, \mathbf{H} - \mathbf{j}^m. \tag{23}$$

The calculation of $\mathbf{j}^m$ is performed by the determination of an additional field on the surface of the unperturbed waveguide such that the electric field parallel to the surface of the perturbed waveguide vanishes.

If the periodic perturbation of a metal waveguide consists of a corrugation of its bottom wall, the height

$2a$ of the guide varies with the position z on the axis

$$2a(z)=2a(z+L)=2a+\tilde{a}_1\cos(2\beta_0 z)+\ldots+\ldots, \quad (24)$$

where $\tilde{a}_1$ indicates the first Fourier coefficient. For a triangular corrugation of depth $2a_1$ this coefficient is $\tilde{a}_1=8a_1/\pi^2$.

Under these circumstances (23) implies a surface current $\mathbf{j}^m$ [29]

$$\mathbf{j}^m=\mathbf{n}\times[Z_0 ikl(\mathbf{n}\times\mathbf{H})+\mathrm{grad}(\mathbf{E}\cdot\mathbf{n}l)]. \quad (25)$$

$\mathbf{n}$ is normal to the surface of the unperturbed waveguide. l represents the perturbation

$$\begin{aligned} l&=\tilde{a}_1\cos(2\beta_0 z) \quad \text{on the corrugated surface},\\ l&=0 \qquad\qquad\quad \text{on all other surfaces}. \end{aligned} \quad (26)$$

The coefficients $c_\pm(z)$ of the orthonormalized modes (5) are related to this surface current by the integral [29]

$$4\cdot dc_\pm/dz=\mp\oint\mathbf{j}^m\mathbf{H}_\pm^* ds, \quad (27)$$

where the integration is carried out over the unperturbed waveguide profile in the x,y-plane perpendicular to the waveguide axis z. The coupled-wave equations (9) can be deduced from (26 and 27) by neglecting terms of the order l^2. This yields the following coupling coefficients:

$$\kappa_+=\kappa_-^*=\kappa=-e^{-2i\Delta z}\cdot(k/4Z_0)\times\oint l[Z_0^2(\mathbf{H}_{+,s}^*\mathbf{H}_{-,s}+\mathbf{H}_{+,z}^*\mathbf{H}_{-,z})-\mathbf{E}_{+,n}^*\mathbf{E}_{-,n}]\,ds. \quad (28)$$

The index z denotes the field in z direction, the index s the field perpendicular to z and parallel to the surface, and the index n the field normal to the surface.

For a hollow waveguide of rectangular cross section (28) yields a selection rule for the transverse mode numbers $m_\pm$ of the propagation constants $\beta_\pm$ (15 and 16)

$$|m_+|=|m_-|=m. \quad (29)$$

In the following we restrict the considerations to $\mathrm{TM}_{mn_+}-\mathrm{TM}_{mn_-}$ couplings, since in the case of rectangular waveguides only these modes couple efficiently [16, 30]. For these couplings the coefficients κ is given by

$$\kappa=f\frac{\tilde{a}_1}{4a}\cdot\frac{k^2+|\beta_+\beta_-|}{(|\beta_+\beta_-|)^{1/2}}, \quad (30)$$

where the factor f is defined by

$$f=\{[1+(ma/n_+b)^2][1+(ma/n_-b)^2]\}^{-1/2}. \quad (31)$$

For $ma\ll n_\pm b$ this factor is approximately one.

The determination of the coupling coefficients (30) for the corrugated hollow metal waveguide is the relevant feature of the coupled-wave theory presented. Naturally, several approximation had to be made to obtain the simple coupling constant κ represented by (30 and 31). Nevertheless, this coupling constant is in remarkable agreement with the measurements discussed in Sects. 6 and 7.

3. Dispersion Relations and Resonance Conditions for Continuous DFB Structures

3.1. Dispersion Relations of Infinite DFB Structures

The dispersion relations of DFB structures with index and/or gain modulation have been studied in detail and reviewed by Kogelnik and Shank [20], Affolter and Kneubühl [16], Preiswerk et al. [26], Gnepf and Kneubühl [22]. These dispersion relations are relevant for the resonance conditions of DFB lasers which are discussed in the following Sect. 3.2. The context between dispersion and resonance conditions is demonstrated in Sect. 3.3. With respect to these considerations it should be emphasized that dispersion relations hold for infinite DFB structures, while resonance conditions refer to finite DFB structures.

Standard dispersion relations connect the propagation constant of a wave in a medium or in a waveguiding structure with the circular frequency ω or free-space wavenumber k. Examples are the dispersion relation $\beta_{mn}(k)$ of the unperturbed modes mn of the metal waveguide, (15), and the function $\gamma(\Delta)$ of a DFB

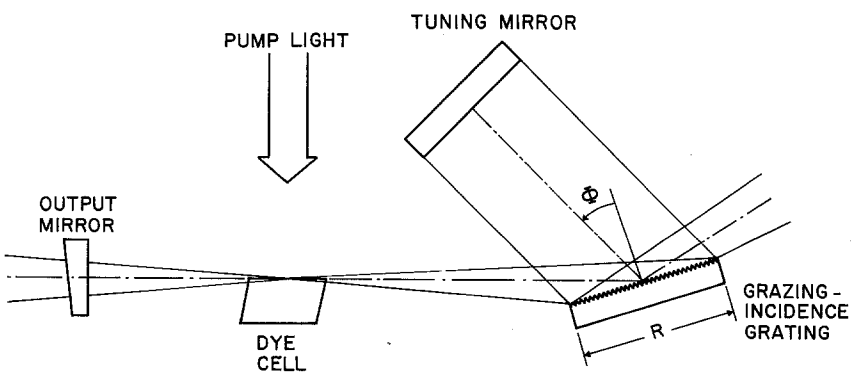

Fig. 1. Schematic view of a grazing-incidence dye laser

structure derived from coupled-wave theory, (14). In our experiments, however, the frequency ω and the wavenumber k can be assumed constant, because we work with the optically pumped 496 μm CH_3F emission which exhibits a strong laser action due to a pure rotational transition [19]. This FIR laser transition is homogeneously broadened by 40 MHz/Torr at pressures above 50 mTorr [65]. This implies a gain bandwidth of about 150 MHz in our actual 496 μm CH_3F laser. For this reason we tune the laser by a variation of the cross section of its waveguide. Consequently, we consider the propagation constants as functions of the waveguide height $a_0 = 2a - a_1$ instead of the wavenumber k. For this purpose we replace $\beta_{mn}(k)$ by $\beta_{mn}(k = \text{const}, a_0)$ in (15) and $\gamma(\Delta)$ by $\gamma(k = \text{const}, a_0)$ in (14). This allows us a more convenient comparison of theory and experiment.

In order to compare the dispersions of the unperturbed and perturbed waves we consider the complete propagation constants $\tilde{\beta}(a_0)$ of the forward and backward eigenwaves in the corrugated waveguide. According to (5, 10–12, and 14) $\tilde{\beta}(a_0)$ is defined by

$$\tilde{\beta}_{\pm}(a_0) = \beta_{\pm}(a_0) \pm [\gamma(a_0) - \Delta(a_0)]. \tag{32}$$

For a vanishing perturbation, i.e. $\kappa_{\pm} = 0$, (32) reduces to

$$\tilde{\beta}_{\pm}(a_0) = \beta_{\pm}(a_0) \pm i\alpha. \tag{33}$$

This represents the propagation constant of an unperturbed forward or backward wave with gain α.

In general, both, the forward wave $\tilde{\beta}_+$ and backward wave $\tilde{\beta}_-$, are required to describe the fields in the corrugated waveguide and thus, to determine the dispersion relation. In addition, the determination of the resonance condition of the finite corrugated structure in Sect. 3.2 involves the definition of a round-trip condition of the optical path. This is accomplished by a summation of the phases of the two counterpropagating waves which are determined by the propagation constants $\tilde{\beta}_{\pm}$. Therefore, it was found convenient to introduce a modified propagation constant β which is defined as

$$\begin{aligned}\beta(a_0) &= [\tilde{\beta}_+(a_0) - \tilde{\beta}_-(a_0)]/2 \\ &= \beta_0 + \gamma(a_0) = (\pi/L) + \gamma(a_0)\end{aligned} \tag{34}$$

or

$$\beta(a_0) \cdot (L/\pi) = 1 + \gamma(a_0)(L/\pi). \tag{35}$$

Both equations hold for the first-order Bragg or DFB resonance defined by the Bragg wavenumber $\beta_0 = \pi/L$.

For a passive waveguide structure with $\alpha = 0$ the real part of the dispersion relation exhibits the well-known stopband at β_0. Lower and upper boundaries of this gap are determined by the coupling coefficient κ with the relation

$$\Delta = \pm\kappa. \tag{36}$$

In Fig. 2 we show the real and imaginary part of the dispersion relation (35) of the passive waveguide for three different mode-couplings, i.e. $TM_{11}-TM_{11}$, $TM_{11}-TM_{12}$, and $TM_{12}-TM_{12}$. This dispersion relation has been calculated for a spacing of the periodic corrugations of $L = 0.255$ mm and a free-space wavelength $\lambda = 0.496$ mm. These parameters correspond to the experiments described in Sects. 6 and 7. The flash where $\beta L/\pi = 2L/\lambda$ indicates the free-space wavenumber $\beta = k$. This value cannot be exceeded.

Figure 3 shows the dispersion relation of the same mode-couplings as Fig. 2, but with a positive gain α.

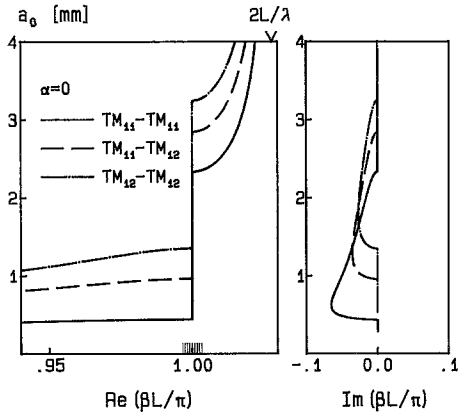

Fig. 2. Dispersion relation of a passive ($\alpha = 0$) rectangular periodic waveguide. The normalized propagation constant $\beta L/\pi$ is plotted as a function of the waveguide height a_0 for different mode couplings. The grating period is $L = 0.255$ mm, and the free-space wavelength $\lambda = 0.496$ mm

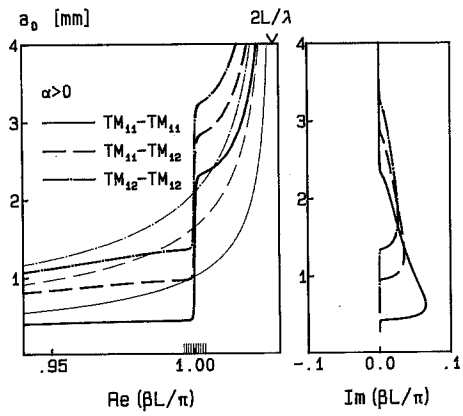

Fig. 3. Dispersion relation of an active ($\alpha > 0$) rectangular periodic waveguide. The normalized propagation constant $\beta L/\pi$ is plotted as a function of the waveguide height a_0 for different mode couplings. The grating period is $L = 0.255$ mm, and the free-space wavelength $\lambda = 0.496$ mm. The thick lines indicate low gain ($\alpha = 0.05\ \text{cm}^{-1}$), while the thin lines correspond to high gain ($\alpha = 10\ \text{cm}^{-1}$)

For the limit of the low-gain approximation ($|\alpha| \ll \kappa$), indicated by thick lines, the real part of β shows no significant change. Only the sign of the imaginary part of β changes. For the limit of the high-gain approximation ($|\alpha| \gg \kappa$), indicated by the thin lines, the characteristic stopband disappears completely, and the dispersion relation approaches that of a unperturbed waveguide. The intersection of the low- and the high-gain curves indicates the center of the stopband, i.e. $\Delta = 0$.

3.2. Resonance Conditions of Finite Structures

On the basis of the general solution of the coupled-mode equations (12) we derive a resonance condition as follows: The corrugated waveguide has a finite length R from $z=0$ to $z=R$. We assume that no input waves at $z=0$ and $z=R$ are admitted, i.e. that $A_+(z=0) = A_-(z=R)=0$ (12). If we take into consideration the boundary conditions for $A_\pm(z)$ at $z=0$ and $z=R$, we find the following resonance condition [22, 30]

$$s^2 \exp(-2i\gamma R) = \exp(-2\pi i q), \tag{37}$$

where according to (13, 28, and 30), s is given by

$$s^2 = s_+ s_- . \tag{38}$$

The integer q denotes the DFB mode number. In the resonance condition (37) constant phases are neglected. It has been derived by assuming self-consistency which implies that the DFB cavity yields an output without admitting an input. This corresponds to a self-consistent oscillation.

Approximations of (37) can be deduced for the limits of high and low threshold gains. For the high-gain approximation with $|\alpha| \gg \kappa$ we obtain from (14) an approximate expression for γ

$$\gamma = \Delta + i\alpha . \tag{39}$$

A comparison of the absolute values of (37 and 39) results in the threshold condition [20]

$$\kappa = 2\alpha e^{\alpha R} \tag{40}$$

while a comparison of the phases gives the resonance condition for high threshold gain [16, 18, 20, 38–42]:

$$R \cdot \Delta(a_0) + \tfrac{\pi}{2} = q\pi \tag{41}$$

or

$$R[\beta_+(a_0) - \beta_-(a_0)] = \pi(rM + q + 1/2). \tag{42}$$

In this condition r indicates the DFB order, q the DFB mode number, and $M = R/L$ the number of corrugations. For a wedged waveguide applied in a grazing-incidence gas laser [38–42] the left side of (42) has to be replaced by an integral according to (17)

$$\int_0^R (\beta_+ - \beta_-) dz = \pi(rM + q + 1/2). \tag{43}$$

This integration allows us to eliminate the z-dependence of the propagation constant (Sect. 2.3).

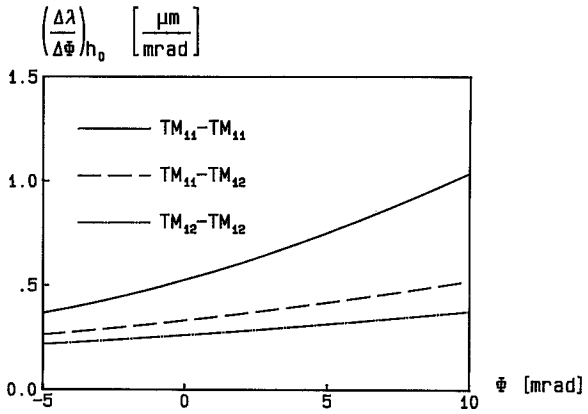

Fig. 4. $(\Delta\lambda/\Delta\Phi)$ versus tuning angle Φ for different high-gain mode couplings

This integration allows us to eliminate the z-dependence of the propagation constant (Sect. 2.3).

In order to demonstrate the influence of the tuning angle Φ on the resonant wavelength we have calculated the relations between the variation $\Delta\Phi$ and the corresponding change $\Delta\lambda$ of the emission wavelength. These calculations are based on the high-gain approximation (43). The height $h_0 = a_0 + R \cdot \Phi$ is kept constant according to the design of the experiment (Sect. 5). Figure 4 shows this relation for axial mode number $q=0$ and the symmetrical mode couplings $TM_{11}-TM_{11}$, $TM_{12}-TM_{12}$, and the asymmetrical coupling $TM_{11}-TM_{12}$. These curves are valid for first-as well as for second-order DFB because the halving of the number M of corrugations compensates the doubling of the corrugation spacing L.

In order to derive approximate resonance conditions for low threshold gain, respectively high feedback characterized by $|\alpha| \ll \kappa$, we first evaluate the eigenvalue γ (14)

$$\gamma = (\operatorname{sgn}\Delta)\,\kappa(2\varepsilon)^{1/2} + i\alpha(2\varepsilon)^{-1/2}, \tag{44}$$

where

$$\varepsilon = |\Delta|/\kappa - 1 \ll 1 \tag{45}$$

is supposed to be small. This implies that the resonances are close to the stopband boundaries. With the assumption that $\kappa \cdot R \gg (2\varepsilon)^{1/2} \simeq 0$, the resonance condition (37) can be written as [30, 31]

$$q\pi = R\gamma_0(a_0), \tag{46}$$

where γ_0 is the real part of γ in (14). The threshold gain α_q depends on the DFB mode number q. It is deter-

mined by

$$\alpha_q=(q\pi/\kappa)^2R^{-3} \tag{47}$$

for a given q resonance. For a grazing-incidence laser, the expression $(\beta_+-\beta_-)$ implicitly included in (46) needs to be replaced by the integral (17) as demonstrated for the case of high threshold gain (43).

In contrast to the high-gain approximation the resonance condition (46) still depends on the coupling coefficient κ. This is reasonable since the low-gain approximation corresponds to the case of the passive resonator, whose dispersion relation is strongly influenced by κ (Fig. 2).

3.3. Relations Between Dispersion and Resonance Conditions

For a vanishing tuning angle $\Phi=0$, the resonance conditions (41 and 46) can be interpreted graphically with the aid of the dispersion relations plotted in Figs. 2 and 3.

By multiplying the dispersion relation (34) by R we can write for the low-gain approximation (46)

$$\mathrm{Re}\{\beta\}\cdot R=\pi R/L+\gamma_0 R=\pi R/L+q\pi \tag{48}$$

or

$$\mathrm{Re}\{\beta\}\,(L/\pi)=1+(qL/R)=1+(q/M), \tag{49}$$

Therefore, the resonant heights a_r can be evaluated by scaling the axis $(\mathrm{Re}\beta)(L/\pi)$ around 1 with q/M, where $q=0,\pm1,\pm2,\pm3\ldots$. For the low-gain limit this has been done in Fig. 2 in order to show the separation between two neighbouring resonances.

For the limit of the high-gain approximation (41) the dispersion relation indicated by thin lines in Fig. 3 is relevant for the determination of the resonant heights a_r, because these curves correspond to the dispersion of an unperturbed waveguide. With respect to the low-gain approximation the equidistant intervals are shifted by $1/2M$

$$\mathrm{Re}\{\beta\}\,(L/\pi)=1+(q+1/2)/M. \tag{50}$$

On the normalized β-axis the separations between two adjacent axial modes defined by q agree for both approximations. On the other hand, the difference between two adjacent resonant heights a_r is much smaller for the low-gain approximation.

4. Resonance Conditions for DFB Structures with a Gap

The high- and low-gain approximations of the dispersion relations and resonance conditions of Sect. 3 for continuous DFB structures reveal the absence of laser resonances inside the stopband of the dispersion relation. Resonances inside the stopband have an advantage over those outside because they involve a higher feedback [29]. They can be realized by the introduction of an additional phase-shifting component, e.g. by a variable gap D in the center, i.e. at $z=R/2$, of the otherwise continuously periodic DFB structure. This yields a laser oscillation near the Bragg frequency [27, 30, 31]. In addition, the gap provides a controllable discrimination between the individual laser modes, which allows single-mode operation of the DFB gap laser [27, 33].

The boundary conditions for $A_\pm(z)$, (12), at the gap and at the ends of the DFB laser, i.e. at $z=0$, $R/2$, $R/2+D$, $R+D$ imply the following resonance conditions

$$\exp[-\mathrm{i}(\beta_+-\beta_-)D]\frac{s^2[1-\exp(-\mathrm{i}\gamma R)]^2}{[1-s^2\exp(-\mathrm{i}\gamma R)]^2}=\exp(-2\pi\mathrm{i}N), \tag{51}$$

where N is an integer. For $D=0$ this general resonance equation corresponds to the resonance condition (37) of the DFB laser without gap.

An approximative resonance condition for the limit of low threshold gain is obtained by a comparison of the phases in (51). Inside the stopband γ is imaginary. Thus, we define for $\alpha\simeq0$

$$\tilde{\gamma}=\mathrm{i}\gamma=(\kappa^2-\Delta^2)^{1/2}. \tag{52}$$

If we eliminate s^2 in (51) with the aid of (13 and 38) we find

$$2\pi N+(\beta_+-\beta_-)D=2\cdot\mathrm{arctg}\frac{\tilde{\gamma}[1+\exp(-\tilde{\gamma}R)]}{\Delta[1-\exp(-\tilde{\gamma}R)]}. \tag{53}$$

The integer N indicates that the resonances are 2π periodic. For the center of the stop band where $\Delta=0$ the phase $\phi=(\beta_+-\beta_-)D$ is equal π. For a laser oscillation near the Bragg frequency the gap D fulfils therefore the following approximate resonance condition

$$D\simeq(p+1/2)(\lambda_{\mathrm{guide}}/2),\quad p=0,1,2,3,4,\ldots. \tag{54}$$

The threshold gain α as a function of the gap D cab be evaluated by a comparison of the absolute values of the left and the right side of (51). However, due to the high reflection coefficient of the structure near the Bragg frequency [27, 30] the threshold gain is very low and cannot be determined analytically. Hence in a first approximation the threshold gain α is of the order of the waveguide losses determined by (20 and 21).

5. Design and Operation of the Laser

In this chapter we report on the design and the operational characteristics of the DFB and grazing-incidence optically pumped 496 μm CH_3F laser. The first section is devoted to the design of the specific laser cavity, the second to the general experimental arrangement, and the third to the transverse mode pattern of the pump beam which is relevant for our experiments described in Sects. 6 and 7. Finally, in the last section we discuss the experimental procedures applied in our investigations.

5.1. The Laser Cavity

Most features of our DFB and grazing-incidence optically pumped 496 μm CH_3F laser agree with those of our previous DFB CH_3F laser published by Affolter and Kneubühl [15–17]. The main difference is a new cavity which is illustrated in Fig. 5a. It consists of a special rectangular metallic waveguide of length $R=300$ mm, whose bottom wall is formed by an exchangable grating mounted in a dovetailed guide. The top wall, which represents the tuning mirror, is plane and can be rotated by a small angle Φ with respect to the grating. In addition, the height h_0 of the cavity can be varied between 0 and 10 mm. The adjustable height h_0 allows the cavity to be tuned over a wide frequency range while the slight variation of the angle Φ permits fine tuning (Sect. 2.3). The side walls, the tuning mirror and the grating of the hollow metallic cavity are covered with gold by vapor deposition in order to prevent surface oxidation. The gold film has a thickness of at least 0.5 μm which corresponds to 5 times the skin depth of an electromagnetic wave with a wavelength of 500 μm.

In order to achieve a higher feedback and, consequently, a narrow-band operation of our laser, we have also worked with gratings equipped with a variable gap in the center. The gap allows a continuous correction of any phase mismatch in the roundtrip of the optical path. A schematic view of this modified phase-matched waveguide is shown in Fig. 5b.

In our study we have applied three different gratings with periods $L=250$, 255, and 500 μm which provide first- as well as second-order DFB resonances. The average groove spacing L was measured by means of a projecting microscope with a reading precision of 1 μm. This yields a relative accuracy of $\Delta L/L=10^{-4}$. The determination of an average value of L is reasonable, because small statistical deviations from the correct period cause no significant alteration of the DFB characteristics [66]. All gratings used in our experiments have a blaze angle of 45°. They have been manufactured by diamond cutting or high-speed milling in our workshop.

The entire cavity is mounted in a cell filled with CH_3F at an optimum pressure of 3.5 to 4.5 Torr. The pump beam is coupled into one end of the CH_3F cell through a KCl Brewster window. At the other end we have mounted a quartz window which is transparent only for the FIR radiation.

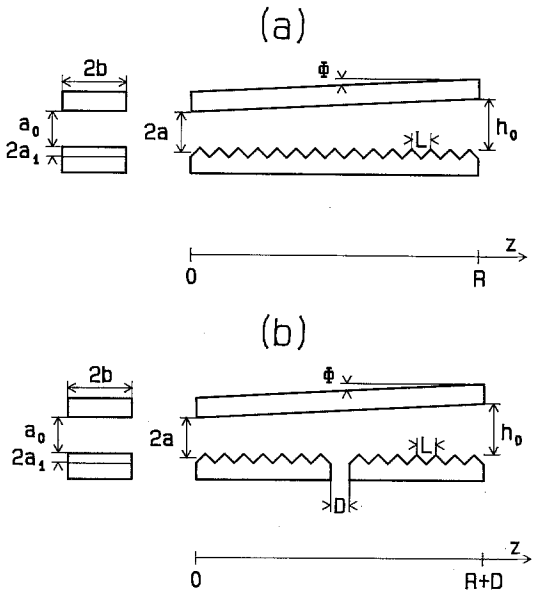

Fig. 5a, b. Schematic view of the FIR cavities, (a) with a continuous grating, (b) with a gap in the center of the grating

5.2. Experimental Arrangement

Our experimental arrangement shown in Fig. 6 is similar to that applied to the study of the first linear periodic DFB [15–17] and HFB [24–26] gas lasers. The stimulated 496 μm CH_3F emission is pumped by the 9.55 μm 9P(20) radiation from a pulsed hybrid CO_2 laser in single-mode operation. The power of the pump pulse is measured by a photon-drag detector PD. It is of the order of several hundred kW. The parallel-polarized pump pulse is focused into the CH_3F cavity by a cylindrical lens CL of focal length 540 mm. The inclinations α and δ, as well as the KCl plate W_1 of the CH_3F cell, serve for the delicate height adjustment of the pump beam. In the course of our experiments, the entrance height of the pump beam relative to the CH_3F waveguide turned out to be relevant and crucial.

The first measurements of the energy of the FIR pulses were made with a Golay detector combined with sample-and-hold electronics. Later, the acquisition of a high-repetition rate (5–20 pps) CO_2 pump laser (PRF 150, Laser Science Inc.) allowed us the application of a pyroelectric detector (ELTEC Instruments, Model 406) directly connected to a lock-in

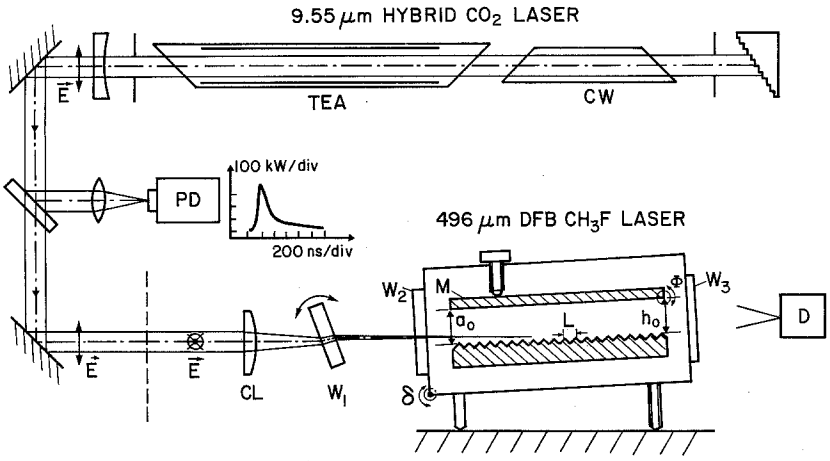

Fig. 6. Experimental arrangement of the grazing-incidence 496 μm CH_3F laser. W_1 indicates a KCl plate, W_2 a KCl window, and W_3 a quartz window

amplifier. Thus, an integration over 5–20 FIR pulses was possible.

5.3. Transverse-Mode Pattern of the Pump Beam

The transverse mode pattern of the pump beam turned out to be a very essential feature of the experiment. Higher transverse modes of the pump beam lead to the stimulation of different and irreproducible mode couplings in the waveguide. For this reason we have developed a low-cost CO_2 laser beam profile monitor [67]. In the monitor a small slit covered by a temperature dependent fluorescent screen is imaged on a photodiode. A rotating mirror scans the spatial intensity distribution over the slit. The signal-to-noise ratio is improved by the repetitive sampling with a low-cost digital processing unit. The high sensitivity of the device permits a real-time surveillance of the spatial beam characteristics with the aid of a beam splitter.

Figure 7 shows an example of a typical transverse mode pattern of the 9.55 μm pump beam measured with our beam profile monitor and used in our experiments. The dashed thin curve represents a Gaussian intensity distribution, which shows that our pump beam intensity distribution corresponds well to a TEM_{00} mode.

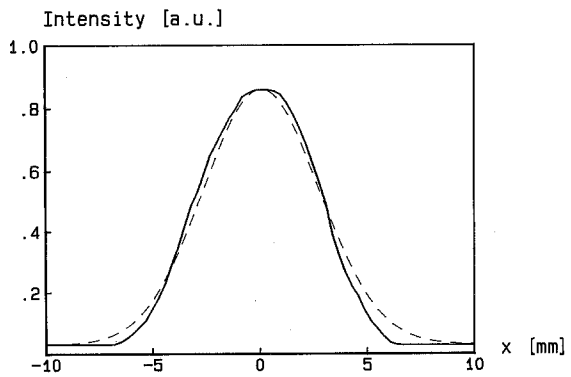

Fig. 7. Measured near-field transverse mode pattern of the 9.55 μm CO_2-laser pump beam. The dashed curve represents a Gaussian intensity distribution

5.4. General Experimental Procedures

In this section we briefly explain the measurement procedures which in general are identical for all gratings and both types of cavities, i.e. those with and without gap.

The single-mode 9.55 μm CO_2 laser pump pulses have an energy of 50–100 mJ and a duration of about 150 ns. The radiation of the pump pulse is polarized parallel to the grooves. The tuning angle Φ of the cavity mirror is scanned from about -2 to $+2$ mrad for a constant cavity height h_0 and gap D in the grating.

The output energy of the FIR emissions is optimized by changing the inclination of the window W_1 and the angle δ shown in Fig. 6. The optimization has no influence on the resonant angles Φ_r. The polarization of the CH_3F emission is perpendicular to the grooves. No parallel-polarized emissions are observed even if the polarization of the pump beam is changed. Thus, we only observe TM mode couplings.

6. Measurements on Laser Cavities Equipped with Continuous Gratings

6.1. Experimental Conditions and Data Presentation

We have succeeded in the first operation of a grazing-incidence 496 μm CH_3F gas laser by means of a cavity equipped with various continuous gratings of different periods L and groove numbers M [37–42]. For these experiments we used a cavity width of $2b=40$ mm which yielded a transverse mode spacing of only 35 MHz. This is considerably less than the CH_3F gain bandwidth of 250 MHz (Sect. 3.1). Hence we did not achieve a proper separation of the transverse modes.

The measurements on our grazing-incidence gas laser described in this chapter have therefore been performed with a reduced cavity width of $2b=10$ mm. Consequently, the transverse mode-spacing has increased to 550 MHz, which implies a considerable improvement with respect to the mode selectivity of our laser.

In order to contrast the measured resonant tuning angles Φ_r and heights a_r with the theory discussed in Sects. 2 and 3, we compare our experimental data with the theoretical resonance conditions (43 and 46) with the aid of $a_0-\Phi$ plots, where a_0 is given by

$$a_0=2a-a_1=h_0-R\Phi; \tag{55}$$

$2a$ is the waveguide height, and $2a_1$ is the groove depth, both defined by (24). h_0 denotes the waveguide height at the waveguide end, i.e. at $z=R=300$ mm. All these geometrical waveguide parameters are shown in Fig. 5.

In the following we describe experiments and the corresponding $a_0-\Phi$ plots for laser cavities with gratings of different selected periods L and groove numbers M. In Sect. 6.2 we compare results obtained for gratings with $L=0.250$ mm and $M=1200$ versus data measured with gratings with $L=0.255$ mm and $M=1176$. Both gratings exhibit first-order DFB, but they reveal drastic differences in their DFB performance. In Sect. 6.3 we present measurements with a grating characterized by $L=0.500$ mm and $M=600$. This grating yields second-order DFB, i.e. proper grazing-incidence laser resonances.

6.2. *First-Order DFB Measurements*

In comparison to our previous measurements [37–42] with cavities of width $2b=40$ mm, we have observed a drastic reduction of the number of the laser resonances for the reduced cavity width $2b=10$ mm. This indicates that the reduced cavity width yields a considerable decrease of the number of the coupled modes. However, Fig. 8 demonstrates that a proper mode separation has not been achieved yet. The resonance presented in Fig. 8 has been measured for a constant height $h_0=2.95$ mm and a grating with $L=0.250$ mm and $M=1200$. Although this resonance is well defined, the sharp peaks on the main emission suggest different mode couplings with respect to the transverse mode number m. Obviously, these couplings cannot be resolved. Figure 9 shows all the observed resonances measured with this grating in an $a_0-\Phi$ plot. The two resonances essentially observed are traced by a variation of the tuning angle Φ. This confirms our theoretical approach with averaged propagation constants (17).

The resonances at a height $a_0\simeq 3$ mm (Fig. 9) can be explained by the high-gain approximation (43),

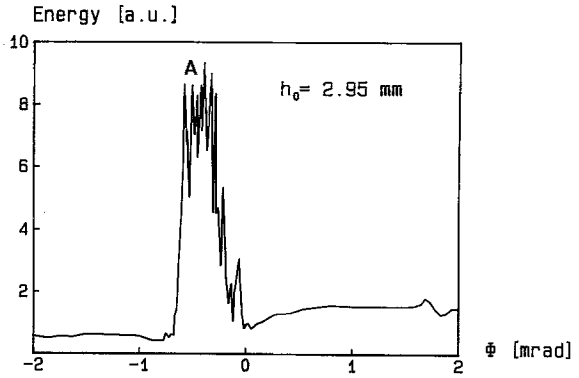

Fig. 8. Example of a resonant first-order DFB 496 μm CH_3F laser emission measured for a cavity with a continuous grating of $M=1200$ grooves and of period $L=0.250$ mm. The angle Φ is scanned at constant cavity height $h_0=2.95$ mm

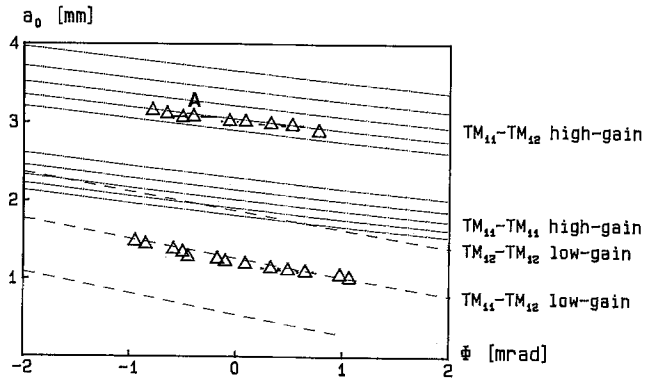

Fig. 9. Comparison of theoretical and experimental first-order DFB resonances for a cavity with a continuous grating of $M=1200$ grooves and of period $L=0.250$ mm. The theoretical curves are calculated with high-gain and low-gain approximations. For high gain the resonance conditions are plotted for the axial DFB mode numbers $q=-2$ to $+2$. For low gain, the axial DFB modes cannot be resolved. The observed resonances are indicated by triangles

which is indicated by dash-dotted curves for the DFB mode numbers $q=0, \pm 1, \pm 2$. $q=-2$ corresponds to the lowest curve of the respective mode coupling $TM_{mn+}-TM_{mn-}$. The specific resonance "A" indicated in Fig. 8 is also labeled in Fig. 9. The resonances observed at height $a_0\simeq 3$ mm in Fig. 9 correspond to an axial mode number $q=-1$ of the mode coupling $TM_{11}-TM_{12}$.

The high-gain approximation is not adequate for the explanation of the resonances observed at height $a_0\simeq 1.2$ mm in Fig. 9. For decreasing height a_0 the coupling constant κ (30) increases, because the relative perturbation a_1/a of the waveguide increases. This has a direct influence on the feedback capability of a given structure. Due to the higher feedback the threshold gain decreases. Therefore, the low-gain approximation (46) can be applied. It is indicated in Fig. 9 by the

dashed curves. According to the dispersion relation presented in Fig. 2 the resonant heights a_r for different DFB mode numbers q do not change considerably, i.e. they cannot be resolved in our plots. However, the observed resonances can be identified with respect to the transverse mode structure: They occur near the stopband edge of the $TM_{11}-TM_{12}$ coupling.

In order to measure the influence of the groove spacing on the DFB performance of a corrugated waveguide, we have exchanged the cavity grating of period $L=0.250$ mm and groove number $M=1200$ with one of increased period $L=0.255$ mm and correspondingly reduced groove number $M=1176$. In Fig. 10 we present typical resonances observed with these gratings. The scan was made at a constant height $h_0=1.3$ mm. The peaks belong to different axial DFB mode numbers q or to different transverse-mode couplings characterized by m. In the $a_0-\Phi$ plot of Fig. 11 the observed resonances are indicated by triangles. In contrast to the measurements with a grating period $L=0.250$ mm those with the increased period $L=0.255$ mm show many resonances. This can be explained by the smaller separation of different modes which might favour multimode couplings. Another observation supporting this interpretation is the lower sensitivity of the resonances to the incoupling conditions of the pump beam.

In Fig. 11 the theoretical resonance condition based on the high-gain approximation (43) is shown by dash-dotted lines. Only three axial mode numbers q are plotted for each mode coupling, i.e. $q=0, \pm 1$. Again, the specific resonances "A", "B", "C", "D" indicated in Fig. 10 are labeled in the $a_0-\Phi$ plot of Fig. 11. Assuming the threshold gain to be high we can assign these emissions to a transverse $TM_{11}-TM_{11}$ coupling, i.e. the lowest existing coupling.

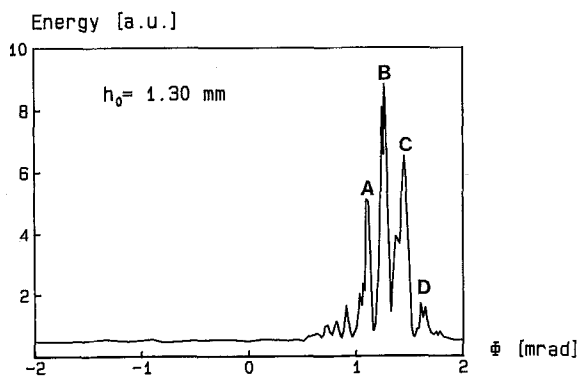

Fig. 10. Examples of resonant first-order DFB 496 μm CH_3F laser emissions measured for a cavity with a grating of $M=1176$ grooves and of period $L=0.255$ mm. The angle Φ is scanned at constant cavity height $h_0=1.30$ mm

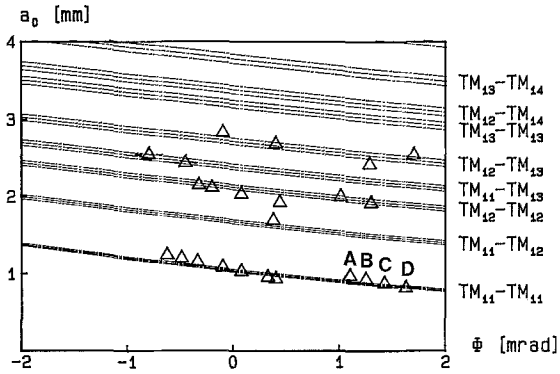

Fig. 11. Comparison of theoretical and experimental first-order DFB resonances for a cavity with a continuous grating of $M=1176$ grooves and of period $L=0.255$ mm. The theoretical curves are calculated with the high-gain approximation and plotted for the axial DFB mode numbers $q=-1, 0, +1$. The observed resonances are indicated by triangles

In summary, the cavity equipped with the grating of period $L=0.250$ mm and groove number $M=1200$ has an advantage over that with a grating defined by $L=0.255$ mm and $M=1176$ with respect to mode selectivity. On the other hand, the enlargement of the grating period L results in a less critical excitation of the resonances. Unfortunately, the axial modes can be identified neither for the shorter nor for the longer period L.

6.3. *Second-Order DFB Measurements*

Our cavity grating of period $L=0.500$ mm and groove number $M=600$ implies second-order DFB laser resonances, because the grating period L corresponds approximately to the emission wavelength $\lambda=496$ μm. The resonances observed with this grating are the proper grazing-incidence resonances. Yet, it should be noticed that they cannot be interpreted by Fraunhofer diffraction as those of standard optical grazing-incidence lasers, since the separation of the diffraction grating from the tuning mirror is only of the order of a few CH_3F laser wavelengths. This implies Fresnel diffraction or waveguiding, as discussed in Sect. 2.

An example of a resonance scan for a cavity height $h_0=1.25$ mm and the grating mentioned above is shown in Fig. 12. It is obvious that the different modes are not resolved. The two observed resonances are labeled by "A" and "B". In Fig. 13 all the observed resonances including "A" and "B" are presented in an $a_0-\Phi$ plot.

The second-order DFB high-gain resonance condition (43) is identical with that of first-order DFB because the halving of the number of grooves is neutralized by the doubled groove spacing. A different coupling phase could shift the theoretical curves

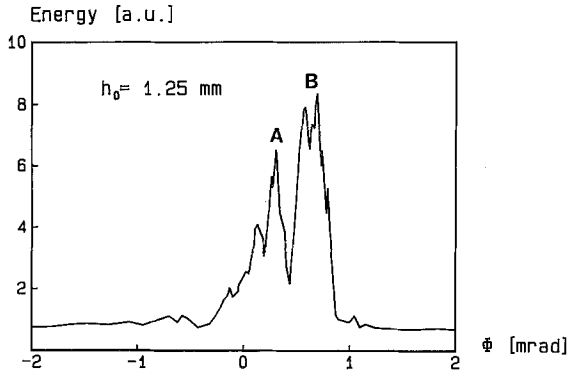

Fig. 12. Examples of resonant second-order DFB 496 μm CH_3F laser emissions measured for a cavity with a grating of $M=600$ grooves and of period $L=0.500$ mm. The angle Φ is scanned at constant height $h_0=1.25$ mm

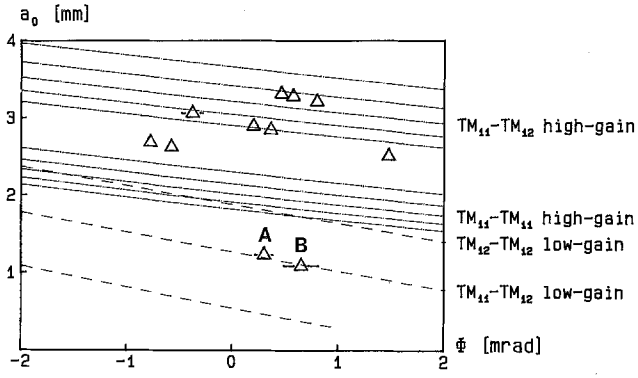

Fig. 13. Comparison of theoretical and experimental second-order DFB resonances for a cavity with a grating of $M=600$ grooves and of period $L=0.500$ mm. The resonance condition is assumed equal to that of first-order DFB represented in Fig. 6.2. The observed resonances are indicated by triangles

unsignificantly. Since our resonances are not identifiable, this shift is irrelevant. The theoretical curves are shown by dash-dotted lines for the axial mode numbers $q=0, \pm 1, \pm 2$.

The low-gain approximation, which is indicated by the dashed curves, is based on the coupling coefficient κ (30) calculated for first-order DFB, because for second-order DFB κ cannot be calculated with present theories. However, assuming a coupling coefficient κ evaluated from first-order DFB theory, we find that the resonances "A" and "B" at a height $h_0=1.25$ mm shown in Fig. 12 correspond to the $TM_{11}-TM_{12}$ coupling as demonstrated in Fig. 13.

In summary, the second-order DFB resonances are as strong as the first-order emissions described in Sect. 6.2, but not all of them can be interpreted by our approximations of the resonance conditions. However, the coupling coefficient κ seems to be of the same order of magnitude since the observed low-gain resonances are in agreement with the first-order DFB resonances.

7. Measurements on Laser Cavities with a Gap in the Grating

7.1. Purpose and Data Presentation

Rapidly increasing bit rates and transmission distances made possible by improvements in the performance of optical fibers require laser diodes with very stable, single logitudinal mode output [68, 69]. As proposed in Sect. 4, a gap in the center of the corrugation can remove the mode degeneracy of conventional semiconductor DFB lasers working at optical and near infrared wavelengths. In order to investigate the characteristics of such phase-matched DFB lasers in a wavelength region better suited for detailed experimental studies we have realized the first FIR DFB gas laser with a variable gap D in the center of the corrugation [43, 70].

As demonstrated in Sect. 6, the mode separation of different axial modes is very small for a laser cavity with a continuous grating. Therefore, it is not possible to identify the observed resonances in that case. In this chapter we show that the mode separation increases considerably by introducing a gap in the grating.

In the course of our experiments we have made various measurements on laser cavities at a constant waveguide height h_0, but either with a variable gap D in the grating or with a variable angle Φ of the tuning mirror. The resonant gaps D_r measured with an absolute accuracy of 30 μm, the resonant heights a_r, and angles Φ_r are compared with the resonance condition (53). For this purpose we consider $a_0-\Phi$ plots for a constant gap D as well as a_0-D plots for $\Phi=0$.

In Sects. 7.2 and 3 we report on the measurements with gratings of two different periods L and groove numbers M, i.e. $L=0.250$ mm, $M=1200$ and $L=0.255$ mm, $M=1176$. We have also performed experiments on second-order DFB with gratings of period $L=0.500$ mm and groove number $M=600$ with a variable gap D. The observed resonances are strong and comparable to first-order DFB emissions. Unfortunately, as already mentioned in Sect. 6.3 the coupling coefficients cannot be calculated by our theory for second-order DFB. Consequently, we cannot describe properly the observed resonances and compare them with theory.

7.2. Measurements with a Grating of Period 0.250 mm

With regard to mode selectivity the best performance of our grazing-incidence gas laser is achieved with a grating of period $L=0.250$ mm and groove number $M=1200$. In order to determine the characteristics of the laser emissions inside the stopband we have scanned first the tuning angle Φ at constant gaps

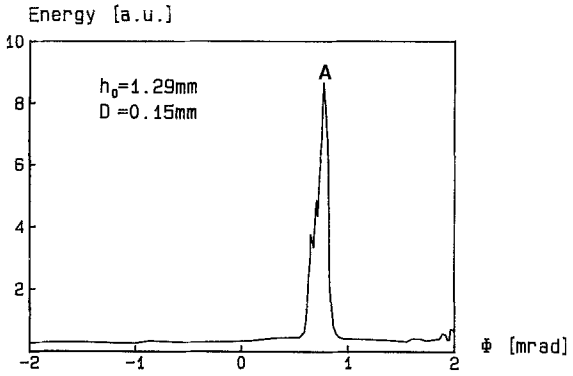

Fig. 14. Example of a first-order 496 μm CH_3F laser emission inside the stop band. The cavity is equipped with a split grating of $M=1200$ grooves and of period $L=0.250$ mm. The angle Φ is scanned at constant cavity height $h_0=1.29$ mm and constant gap $D=0.15$ mm

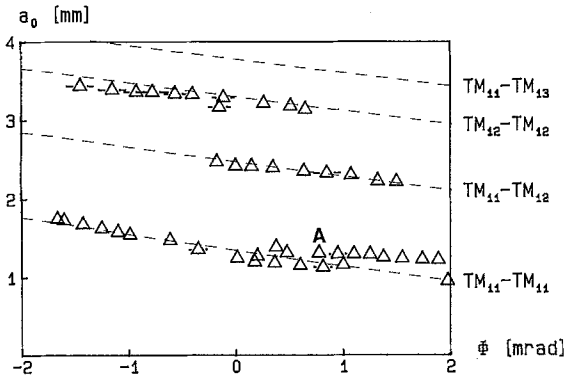

Fig. 15. Comparison of theoretical and experimental first-order DFB resonances for a cavity with a split grating of $M=1200$ grooves, of period $L=0.250$ mm and constant gap $D=0.145$ mm. The measured resonances are indicated by triangles

$D=0.05$, 0.1, 0.15, 0.2, and 0.25 mm. The height h_0 has been varied from 1 to 3.5 mm. We have found only a few well-defined resonances which are very sensitive to the coupling of the 9.55 μm CO_2 laser pump beam into the DFB waveguide cavity. This indicates that the pump beam characteristics are important for the stimulation of the gap modes.

An example of $a_0-\Phi$-scan with fixed gap $D=0.15$ mm is shown in Fig. 14. Due to the higher Q of the phase-matched cavity [27, 30, 33], the full width at half maximum (FWHM) is at least four times smaller than that of a comparable resonance measured with a continuous grating defined by $D=0$. The constant gap $D=0.150$ mm corresponds to a phase shift $\phi \simeq 6\pi/5$ per round trip which indicates that the observed resonance "A" occurs near the Bragg frequency.

Figure 15 shows all the observed resonances in the $a_0-\Phi$ plot for a measured gap $D=0.150$ mm. The best fit of the data is achieved for theoretical curves (53) calculated with an effective gap $D=0.145$ mm. The correction of the gap by -5 μm is well within the limits of accuracy. In addition, we have to reduce the coupling constant κ (30) by a factor of 0.9 in order to achieve better agreement between theory and experiment. However, the calculation of κ is based on a linear approximation. Consequently, the theory predicts a coupling constant only correct to the first power of the waveguide perturbation. Therefore, the agreement between theory and experiment is excellent and gives some confidence in the reliability of the coupled-wave theory. Furthermore, the theory is based on a harmonic perturbation. The triangular grooves of all our gratings have a blaze angle of $\pi/4$. Thus the modulation depth $\tilde{a}_1$ in (30) is determined by the first Fourier coefficient of this triangular modulation (24). This is another source of error which might be noticeable.

Figure 16 shows an example of a D scan for a constant tuning angle $\Phi=0$ and a constant height $a_0=h_0=3.2$ mm. The gap D is scanned from zero to the equivalent of a phase shift $\phi=4\pi$ as indicated on the ϕ axis. The D scan is comparable to a scanning Fabry-Perot measurement since the two half-gratings can be regarded as scanning mirrors. Thus, the observed emission is 2π periodic, and the resonance is repeated after a scan distance of half the guide wavelength λ_g (54). The D-scan measurement demonstrates that the observed resonance is a proper oscillation in the stopband, because for a vanishing gap $D=0$, which corresponds to a grating without discontinuity, no emission is observed.

Figure 17 presents the resonance condition inside the stopband (53) as a function $D(a_0)$ for a tuning angle $\Phi=0$. In order to show all the measured resonances in this plot, the resonant heights a_r of emissions at $\Phi \neq 0$ have been converted into resonant heights a_r' at $\Phi=0$ with the aid of (17). As a consequence, these resonances have been slightly shifted in height according to their

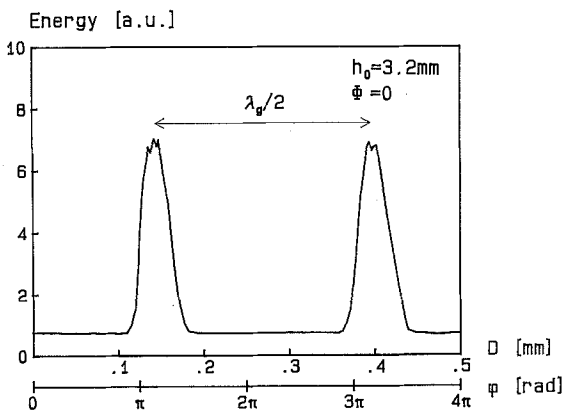

Fig. 16. Example of first-order 496 μm CH_3F laser emissions inside the stop band. The cavity is equipped with a split grating of $M=1200$ grooves and of period $L=0.250$ mm. The gap D is scanned at constant cavity height $h_0=3.2$ mm and constant tuning angle $\Phi=0$

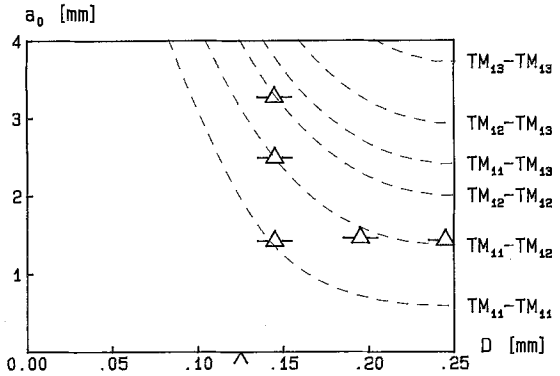

Fig. 17. Comparison of theoretical and experimental first-order DFB resonances inside the stop band for a cavity with a split grating of $M=1200$ grooves, of period $L=0.250$ mm and constant tuning angle $\Phi=0$. The measured resonances are indicated by triangles. The flash on the D-axis indicates the stopband center

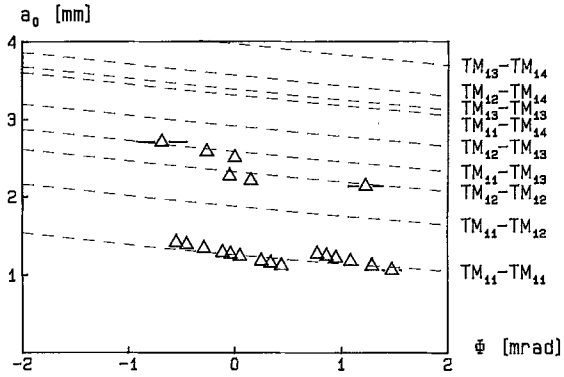

Fig. 18. Comparison of theoretical and experimental first-order DFB resonances inside the stop band for a cavity with a split grating of $M=1176$ grooves, of period $L=0.255$ mm and constant gap $D=0.105$ mm. The measured resonances are indicated by triangles

resonant angle Φ_r. This yields the five main resonances specified in Fig. 17. The indicated three resonances at a gap $D_r=0.145$ mm are the converted resonances of Fig. 15. The low-gain approximation (46) for homogeneous gratings agrees with the resonance condition (53) for a cavity grating with gap, if the phase-shift ϕ caused by the gap D is equal to $N\cdot 2\pi$. Hence, the observed resonance explained by the low-gain approximation in Fig. 9 is also indicated in Fig. 17.

In summary, we have succeeded in observing modes inside the stop band by introduction of a gap in the cavity grating. Their well-defined separation agrees with our theory and results in single-mode operation of the laser.

7.3. *Measurement with a Grating of Period 0.255 mm*

For a grating with period $L=0.250$ mm, the resonance condition strongly depends on the gap D in the region of the stopband center, as demonstrated by the theoretical curves in Fig. 17. This might imply the already mentioned high sensitivity to the coupling of the 9.55 μm CO_2-laser pump beam into the waveguide cavity. Therefore, we have replaced the grating of period $L=0.250$ mm and groove number $M=1200$ by that of period $L=0.255$ mm and groove number $M=1176$. This decreases the stopband width by a factor of one fourth. As a consequence the influence of the gap D is reduced.

Figure 18 shows the theoretical curves and the strongest of the observed resonances, indicated by Δ's for a constant gap $D=0.105$ mm, while Fig. 19 presents the D-scan measurements. It should be noticed that due to the enlargement of the groove spacing L by $+5$ μm, the theoretical mode separation has decreased drastically. Therefore, the number of the observed resonances has increased. Again we have fitted theory with measurements by a correction of the resonant

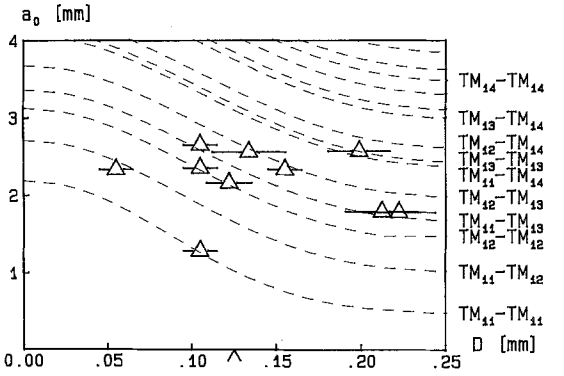

Fig. 19. Comparison of theoretical and experimental first-order DFB resonances inside the stop band for a cavity with a split grating of $M=1176$ grooves, of period $L=0.255$ mm and tuning angle $\Phi=0$. The measured resonances are indicated by triangles. The flash on the D-axis indicates the stopband center

gaps D_r by $+5$ μm and by multiplying the theoretical coupling constant κ by a factor 0.9.

In contrast to the measurements with the grating of period $L=0.250$ mm not all the observed resonances can be explained by the coupled-wave theory. Due to the smaller mode separation more than two counterpropagating modes may couple. Thus, our restriction to a two-mode coupling is no more justified. Naturally, a multimode coupling cannot be treated analytically by simple procedures, because in first-order approximation it corresponds to an eigenvalue problem of a $n\times n$ matrix. However, the strongest of the observed resonances fit well with theory. This indicates that the threshold gain for multimode couplings is considerably higher than that for two-mode couplings.

8. Conclusions

We have performed theoretical and experimental studies on standard and phase-matched DFB and

grazing-incidence gas lasers. On the basis of the coupled-wave theory and the characteristics of metal waveguides we have derived dispersion relations and resonance conditions for these lasers. Furthermore, we have presented a coupled-wave theory which allows an approximative calculation of the coupling coefficients for corrugated metal waveguides. For the case of a rectangular waveguide we have calculated the TM-coupling coefficients and compared them with literature.

In experiment, we have realized the first optically pumped 496 μm CH_3F grazing-incidence laser. Its cavity consists of a hollow rectangular metallic waveguide whose bottom is formed by a grating which provides first- or second-order DFB. The tuning mirror acts as a top of this waveguide. We have measured the resonant tuning angles Φ_r and heights a_r of our laser with three different continuous gratings. The best performance with respect to mode selectivity has been achieved with a grating with $M=1200$ grooves and a groove spacing $L=0.250$ mm. In order to improve the mode selectivity and to decrease the bandwidth of our FIR CH_3F laser we have introduced a variable gap in the center of the grating which serves for phase matching. For this configuration we have achieved single-mode operation of our DFB laser because the gap in the grating yields a considerable increase of the mode separation.

From our experiments we infer that the pump beam geometry of the single mode 9.55 μm CO_2 laser is an important feature, because the region of excited CH_3F in the waveguide strongly depends both on the transverse mode pattern and on the incoupling conditions. This phenomenon is enhanced with increasing mode separation, which suggests that the intensity distribution of the stimulated coupled modes should coincide with the pumped waveguide region. This condition represents a selection mechanism for the oscillation of the waveguide modes.

We have furthermore compared the resonances observed with continuous gratings with high and low threshold gain approximations of the resonance condition derived from the coupled-wave theory. For this purpose we have contrasted the observed resonant tuning angles Φ_r and heights a_r with the theoretical resonance conditions. Most of the observed resonances have been identified with respect to the transverse mode number n. However, it was not possible to identify the DFB mode number q because the mode separation of adjacent q's is too small.

For cavities phase-matched by a variable gap in the grating we have compared the heights a_r, angles Φ_r and gaps D_r of the resonances inside the stopband with the resonance equation adapted to phase matching. For a grating with period $L=0.250$ mm and $M=1200$ grooves all the observed resonances have been identified with respect to the transverse mode numbers m, n. On the other hand, it was not possible to identify all observed resonances for a grating of period $L=0.255$ mm and $M=1176$ grooves. The smaller mode separation provided by this grating probably implies multimode couplings.

The excellent agreement of the measured gap modes with the perturbation theory in the case of a grating period $L=0.250$ mm and $M=1200$ grooves allows the conclusion that a large mode separation is an indispensible requirement for the application of a coupled-mode theory restricted to two modes. Furthermore, the gap in the center of the grating yields a high-feedback performance of the DFB structure. However, in order to attain an optimum laser output power, the net gain of the laser has to be related to the reflection coefficient of the structure. As a consequence, an additional selection mechanism for the oscillation of certain coupled modes is provided by the gap width D, because its variation permits an alteration of the feedback characteristics of the structure.

Investigations on DFB semiconductor lasers with constant $\frac{\pi}{2}$ phase matching have demonstrated an improvement of the characteristics with respect to mode selectivity. The mode degeneracy typical for conventional DFB lasers can be eliminated. Our investigations demonstrate that a variable phase matching in the center of a DFB structure would allow an even more advantageous performance of laser diodes, e.g. by the optimization of output power, the reduction of bandwidth, and the improvement of frequency tuning.

In conclusion, it should be mentioned that the study of DFB and grazing-incidence far-infrared gas lasers provides detailed information on the influence of the various grating parameters on the characteristics of all types of DFB lasers.

Acknowlwdgements. The authors wish to thank Z. Bor, Szeged, H; R. Brönnimann, Murray Hill, US; R. Dändliker, Neuchâtel, CH; H. Kogelnik, Holmdel, US; V. S. Letokhov, Troitzk, USSR; C. V. Shank, Holmdel, US; E. A. Tikhonov, Kiev, USSR; and Shyh Wang, Berkeley, US, for stimulating discussions and suggestions. In addition, we are indebted to X. Zheng, Guangzhou, PRC; J. Arnesson, P. P. Herrmann, W. Leuthard, W. Rüegsegger for experimental assistance, E. Hausammann, G. Schürch for technical support, and Mrs. D. Anliker for typing the manuscript.

This study was supported by the Swiss National Science Foundation and by ETH Zürich.

References

1. I. Shoshan, N. Danon, U. Oppenheim: J. Appl. Phys. **48**, 4495–4497 (1977)
2. M.G. Littman: Opt. Lett. **3**, 138–140 (1978)

3. M.G. Littman, H.J. Metcalf: Appl. Opt. **17**, 2224–2227 (1978)
4. T.W. Hänsch: Appl. Opt. **11**, 895–898 (1972)
5. S. Saikan: Appl. Phys. **17**, 41–44 (1978)
6. S.G. Dinev, I.G. Koprinkov, K.V. Stamenov, K.A. Stankov: Opt. Commun. **32**, 313–316 (1980)
7. S.G. Dinev, I.G. Koprinkov, K.V. Stamenov, K.A. Stankov: Appl. Phys. **22**, 287–291 (1980)
8. K. Lin, M.G. Littman: Opt. Lett. **6**, 117–118 (1981)
9. M.G. Littman: Appl. Opt. **23**, 4465–4468 (1984)
10. P. McNicholl, H.J. Metcalf: Appl. Opt. **24**, 2757–2761 (1985)
11. H. Kogelnik, C.V. Shank: Appl. Phys. Lett. **18**, 152–154 (1971)
12. C.V. Shank, J.E. Bjorkholm, H. Kogelnik: Appl. Phys. Lett. **18**, 395–396 (1971)
13. M. Nakamura, A. Yariv, H.W. Yen, S. Somekh, H.L. Garvin: Appl. Phys. Lett. **22**, 515–516 (1973)
14. F.K. Reinhart, R.A. Logan, C.V. Shank: Appl. Phys. Lett. **27**, 45–48 (1975)
15. E. Affolter, F.K. Kneubühl: Phys. Lett. **74 A**, 407–408 (1979)
16. E. Affolter, F.K. Kneubühl: IEEE J. QE-**17**, 1115–1122 (1981)
17. F.K. Kneubühl, E. Affolter: "Distributed Feedback Gas Lasers". In *Infrared and Millimeter Waves*, Vol. 5, ed. by K.J. Button (Academic, New York 1982, Chap. 6, 305–337)
18. F.K. Kneubühl: Optica Acta **32**, 1055–1069 (1985)
19. T.Y. Chang, T.J. Bridges: Opt. Commun. **1**, 423–426 (1970)
20. H. Kogelnik, C.V. Shank: J. Appl. Phys. **43**, 2327–2335 (1972)
21. S. Gnepf, F.K. Kneubühl: Int. J. Infrared mmWaves **5**, 667–681 (1984)
22. S. Gnepf, F.K. Kneubühl: "Theory on Distributed Feedback Lasers with Weak and Strong Modulations", in *Infrared and Millimeter Waves*, Vol. 16, ed. by K.J. Button (Academic, New York 1986) Chap. 2
23. S. Gnepf, F.K. Kneubühl: "Strong Periodic and Helical Modulations in DFB Lasers", Proc. Int. Conf. on Lasers' 84, San Francisco (STS Press, McLean, VA 1985) pp. 60–67
24. H.P. Preiswerk, G. Küttel, F.K. Kneubühl: Phys. Lett. **93 A**, 15–17 (1982)
25. H.P. Preiswerk, M. Lubanski, S. Gnepf, F.K. Kneubühl: IEEE J. QE-**19**, 1452–1457 (1983)
26. H.P. Preiswerk, M. Lubanski, F.K. Kneubühl: Appl. Phys. B **33**, 115–131 (1984)
27. R. Shubert: J. Appl. Phys. **45**, 209–215 (1974)
28. H.A. Haus, C.V. Shank: IEEE J. QE-**12**, 532–539 (1976)
29. N.F. Kovalev, I.M. Orlova, M.I. Petelin: Sov. Phys.: Radio Phys. Quant. El. **11**, 449–450 (1968)
30. G.G. Denisov, M.G. Reznikov: Sov. Phys.: Radio Phys. Quant. El. **25**, 407–413 (1983)
31. V.L. Bratman, G.G. Denisov, N.S. Ginzburg, M.I. Petelin: IEEE J. QE-**19**, 282–296 (1983)
32. B.Z. Katsenelenbaum: "Theory of Nonuniform Waveguides with Slowly Varying Parameters". Izd. Akad. Nauk SSR, Moscow, 1961 (in Russian), translated in: FTD-ID(RS)T-0243-79, Foreign Technology Division, WP. AFB, Ohio (1979)
33. S.H. Kim, C.G. Fonstad: IEEE J. QE-**15**, 1405–1408 (1979)
34. K. Sekartedjo, B. Broberg, F. Koyama, K. Furuya, Y. Suematsu: Jpn. J. Appl. Phys. **23**, L791–L794 (1984)
35. C.H. Henry: IEEE J. QE-**21**, 1913–1918 (1985)
36. S.L. McCall, P.M. Platzman: IEEE J. QE-**21**, 1899–1904 (1985)
37. D. Wildmann, R. Furler, H.P. Preiswerk, X. Zheng, F.K. Kneubühl: Helv. Phys. Acta **57**, 256–258 (1984)
38. D. Wildmann, X. Zheng, F.K. Kneubühl: Int. J. Infrared mmWaves **5**, 537–545 (1984)
39. D. Wildmann, X. Zheng, H.P. Preiswerk, F.K. Kneubühl: "Grazing-Incidence Far-Infrared Gas Laser", Proc. Int. Conf. Lasers' 83, San Francisco (STS Press, McLean, VA 1985) pp. 203–206
40. D. Wildmann, X. Zheng, F.K. Kneubühl: "Grazing Incidence FIR Gas Laser", Proc. Int. Conf. Lasers' 84, San Francisco (STS Press, McLean, VA 1985) pp. 68–72
41. X. Zheng, D. Wildmann, F.K. Kneubühl: "Grazing Incidence Waveguide FIR Gas Laser", Proc. 3rd Int. Conf. on Infrared Physics (CIRP 3), Zürich, July (1984) pp. 442–444
42. X. Zheng, S. Gnepf, H.P. Preiswerk, D. Wildmann, F.K. Kneubühl: "Novel Distributed Feedback Gas Lasers" (in Chinese). Chinese J. Infrared Res. **3**, 81–94 (1984)
43. D. Wildmann, F.K. Kneubühl: "Grazing-Incidence FIR Gas Laser", Digest 10th Int. Conf. on Infrared and Millimeter Waves, Lake Buena Vista, FL, USA (1985) pp. 281–282
44. W. Magnus, S. Winkler: *Hills Equation* (Wiley, New York 1966)
45. H.P. McKean, P. van Moerbeke: Invent. math. **30**, 217–274 (1975)
46. H.P. McKean, E. Trubowitz: Appl. Math. **29**, 143–226 (1976)
47. D. Marcuse: IEEE J. QE-**8**, 661–669 (1972)
48. D. Marcuse: *Theory of Dielectric Optical Waveguides* (Academic, New York 1974)
49. H. Kogelnik, C.V. Shank, J.E. Bjorkholm: Appl. Phys. Lett. **22**, 135–137 (1973)
50. S. Wang: J. Appl. Phys. **44**, 767–780 (1973)
51. S. Wang: IEEE J. QE-**10**, 413–427 (1974)
52. S. Wang: Wave Electron. **1**, 31–59 (1974)
53. S. Wang: Appl. Phys. Lett. **26**, 89–91 (1975)
54. A. Yariv: IEEE J. QE-**9**, 919–933 (1973)
55. A. Yariv, A. Gover: Appl. Phys. Lett. **26**, 537–539 (1975)
56. D. Marcuse: Bell. Syst. Tech. J. **48**, 3187–3215 (1969)
57. F.E. Borgnis, C.H. Papas: "Electromagnetic Waveguides and Resonators", in *Encyclopedia of Physics*, Vol. 16, ed. by S. Flügge (Springer, Berlin 1958) pp. 285–422
58. P.M. Lapostolle, A.L. Septier: *Linear Accelerators* (North-Holland Amsterdam 1970) Chap. A.2, p. 22
59. H. Kogelnik: "Theory of Dielectric Waveguides", in *Integrated Optics*, ed. by T. Tamir, Topics Appl. Phys. **7** (Springer, Berlin, Heidelberg 1975)
60. W. Streifer, D.R. Scifres, R.D. Burnham: IEEE J. QE-**11**, 233–253 (1975)
61. A. Yariv, M. Nakamura: IEEE J. QE-**13**, 233–253 (1977)
62. S. Wang: IEEE J. QE-**13**, 176–186 (1977)
63. A. Hardy: IEEE J. QE-**20**, 1132–1139 (1984)
64. W. Streifer, D.R. Scifres, R.D. Burnham: IEEE J. QE-**12**, 74–78 (1976)
65. D.T. Hodges, J.R. Tucker, T.S. Hartwick: Infrared Phys. **16**, 175–182 (1976)
66. J.B. Shellan, P. Agmon, P. Yeh, Y. Yariv: J. Opt. Soc. Am. **68**, 18–27 (1978)
67. D. Wildmann, R. Brönnimann, G. Schürch: Rev. Sci. Instr. **55**, 1777–1778 (1984)
68. M. Kitamura, M. Saki, M. Yamaguchi, I. Mito, Ke. Kobayashi, Ko. Kobayashi: Electron. Lett. **19**, 840–841 (1983)
69. H. Temkin, G.J. Dolan, R.A. Logan, R.F. Kazarinov, N.A. Olsson, C.H. Henry: Appl. Phys. Lett. **46**, 105–107 (1985)
70. D. Wildmann, S. Gnepf, F.K. Kneubühl: Helv. Phys. Acta **59**, 1053–1056 (1986)